A new magneto-cardiogram study using a vector model with a virtual heart and the boundary element method*

Zhang Chen(张 琛)[a)b)], Shou Guo-Fa(寿国法)[c)], Lu Hong(陆 宏)[a)], Hua Ning(华 宁)[a)], Tang Xue-Zheng(唐雪正)[a)], Xia Ling(夏 灵)[c)], Ma Ping(马 平)[b)†], and Tang Fa-Kuan(唐发宽)[a)‡]

[a)] *Department of Cardiology, the 309th Hospital of PLA, Beijing* 100091, *China*

[b)] *Applied Superconductivity Research Center of Peking University, Department of Physics, State Key Laboratory for Artificial Microstructure and Mesoscopic Physics, Peking University, Beijing* 100871, *China*

[c)] *Department of Biomedical Engineering, Key Laboratory for Biomedical Engineering of the Ministry of Education, Zhejiang University, Hangzhou* 310027, *China*

(Received 17 January 2013; revised manuscript received 13 May 2013)

A cardiac vector model is presented and verified, and then the forward problem for cardiac magnetic fields and electric potential are discussed based on this model and the realistic human torso volume conductor model, including lungs. A torso–cardiac vector model is used for a 12-lead electrocardiographic (ECG) and magneto-cardiogram (MCG) simulation study by using the boundary element method (BEM). Also, we obtain the MCG wave picture using a compound four-channel HT_c·SQUID system in a magnetically shielded room. By comparing the simulated results and experimental results, we verify the cardiac vector model and then do a preliminary study of the forward problem of MCG and ECG. Therefore, the results show that the vector model is reasonable in cardiac electrophysiology.

Keywords: magneto-cardiogram, cardiac vector model, boundary element method, realistic human torso

PACS: 07.05.Tp, 07.10.Cm, 87.85.−d **DOI:** 10.1088/1674-1056/22/9/090701

1. Introduction

The magneto-cardiogram (MCG) has been developed for measuring weak magnetic signals by improving superconducting quantum interference device (SQUID) systems and cryogenic or hyperthermia technology.[1] MCG mapping is a promising new noninvasive tool for obtaining functional information concerning the electrical activation of the heart. The technique has been applied in localizing various bioelectric events in the heart, such as the accessory conduction pathway of the Wolff–Parkinson–White (WPW) syndrome.[2,3] However, although the MCG is superior to ECG systems, for example in terms of spatial resolution, its benefits have not received wide recognition from those who are already familiar with the ECG. More efforts are needed in order to make the MCG a standard diagnosis tool.

To improve technical performance, it is effective to develop multichannel systems and to use an MCG in a magnetically shielded room.[4,5] To explore the potential of using the MCG as a diagnostic tool, it is essential to research the numerical methods for medical information analysis, such as the boundary element method (BEM),[6–10] the finite element method (FEM),[11,12] and the finite difference method (FDM),[13] etc. In this paper, we use the BEM to study the electric and magnetic forward problem only for the interfaces between different tissue regions that need to be modeled using this method.

In cardiac studies, cardiac equivalent sources are often used to research the cardiac activities and applied to forward and inverse problems of ECGs and MCGs. The more commonly used heart equivalent sources are equivalent current dipoles (ECDs),[14,15] multiple dipoles, and the equivalent double layer (EDL) source.[16,17] These equivalent sources omit some important information about cardiac electrophysiological behavior and pathological characteristics. Thus, a mathematical model of the cardiac vector model, considered to be a set of nine distributed dipoles which have size and orientation eccentrically placed in the virtual heart, is applied in this paper.

On one hand, we carry out an MCG simulation study using the cardiac vector model by the BEM, based on a virtual heart model and realistic human torso volume conductor. On the other hand, we make MCG measurements using a four-channel HT_c·SQUID in a magnetically shielded room. The results are compared.

2. Theory and method

In biomagnetic forward problems such as in an MCG and an MEG, magnetic field B is caused by electric current in conducting body tissues like the brain and the heart. Magnetic field B and electric potential Φ obey the quasi-static ap-

*Project supported by the State Key Development Program for Basic Research of China (Grant No. 2011CBA00106), the National Natural Science Foundation of China (Grant Nos. 10674006, 81171421, and 61101046), and the National High Technology Research and Development Program of China (Grant No. 2007AA03Z238).

†Corresponding author. E-mail: maping@pku.edu.cn

‡Corresponding author. E-mail: tfk616@yahoo.com.cn

© 2013 Chinese Physical Society and IOP Publishing Ltd

proximation of Maxwell's equations.[18] The electric potential Φ satisfies the Poisson equation with the Neumann boundary conditions in the torso Ω [19]

$$\begin{cases} \nabla\cdot(\sigma\nabla\Phi) = \nabla\cdot\boldsymbol{J}_{\mathrm{P}}, & \text{in} \quad \Omega, \\ \sigma(\nabla\Phi)\cdot\boldsymbol{n} = 0, & \text{on} \quad S_{\mathrm{B}}, \end{cases} \tag{1}$$

where Φ is the electric potential, σ is the tissue-dependent conductivity, $\boldsymbol{J}_{\mathrm{P}}$ is the primary current density, $\boldsymbol{n}$ is the outward normal vector, and S_{B} is the body surface which encloses the volume conductor Ω. The magnetic field B is obtained from the total current density by the Biot–Savart law as

$$B(r) = \frac{\mu_0}{4\pi}\int \boldsymbol{J}(\boldsymbol{r}')\times\nabla\Big(\frac{1}{|\boldsymbol{r}-\boldsymbol{r}'|}\Big)\,\mathrm{d}V', \tag{2}$$

where V is all the active areas, μ_0 is the magnetic permeability of the vacuum, vector $\boldsymbol{r}$ refers to the field point, vector $\boldsymbol{r}'$ to the source point, and $\boldsymbol{J}$ is the current density, containing both the primary current density $\boldsymbol{J}_{\mathrm{P}}$ and the Ohmic volume current density $\boldsymbol{J}_{\mathrm{V}} = -\sigma\nabla\Phi$, which is stimulated by $\boldsymbol{J}_{\mathrm{P}}$.

Magnetic field is calculated for a particular combination of the cardiac equivalent source and the volume conductor. The volume can be considered to be a piecewise homogeneous volume conductor V, which has M different regions. Each region has a constant conductivity σ^k and is bounded by the surface S^k. In this case, applying the divergence theorem to the integral equation (2) leads to[20]

$$\begin{aligned} B(\boldsymbol{r}) \;=\; & B^{\infty}(\boldsymbol{r}) - \frac{\mu_0}{4\pi}\sum_{K=1}^{k}(\sigma_-^k-\sigma_+^k) \\ & \times\int_{S^k}\Phi(\boldsymbol{r}')\nabla\Big(\frac{1}{|\boldsymbol{r}-\boldsymbol{r}'|}\Big)\times\mathrm{d}\boldsymbol{S}^k, \end{aligned} \tag{3}$$

where

$$B^{\infty}(\boldsymbol{r}) = \frac{\mu_0}{4\pi}\int_{V_{\mathrm{M}}}\boldsymbol{J}_{\mathrm{P}}(\boldsymbol{r}')\times\nabla\Big(\frac{1}{|\boldsymbol{r}-\boldsymbol{r}'|}\Big)\,\mathrm{d}V'_{\mathrm{M}}$$

is the magnetic field in an infinite vacuum-like medium due to the primary current density $\boldsymbol{J}_{\mathrm{P}}$, and the electric potential Φ is obtained from the surface integral equation using the Green formulas and boundary conditions for Eq. (1)

$$\begin{aligned} \Phi(\boldsymbol{r}) \;=\; & \frac{\sigma_{\mathrm{s}}}{\overline{\sigma}}\Phi^{\infty}(\boldsymbol{r}) - \frac{1}{4\pi}\sum_{k=1}^{M}(\sigma_-^k-\sigma_+^k) \\ & \times\int_{S^k}\Phi(\boldsymbol{r}')\nabla\Big(\frac{1}{|\boldsymbol{r}-\boldsymbol{r}'|}\Big)\cdot\mathrm{d}\boldsymbol{S}^k, \end{aligned} \tag{4}$$

where σ_-^k and σ_+^k are, respectively, conductivities inside and outside the surface S^k, and $\Phi^{\infty}(\boldsymbol{r})$ is the potential generated by the sources of the field in a finite, homogeneous medium of conductivity σ_{s}. For primary current sources $\boldsymbol{J}_{\mathrm{P}}$ inside a bounded volume conductor, $\Phi^{\infty}(\boldsymbol{r})$ is

$$\Phi^{\infty}(\boldsymbol{r}) = \frac{1}{4\pi}\int_{V_{\mathrm{M}}}\boldsymbol{J}_{\mathrm{P}}(\boldsymbol{r}')\cdot\nabla\Big(\frac{1}{|\boldsymbol{r}-\boldsymbol{r}'|}\Big)\,\mathrm{d}V'_{\mathrm{M}}.$$

However, exact solutions can be obtained only for simple geometrical shapes;[21] an approximate solution $\tilde{\Phi}(x)$ should be given for more realistically shaped surfaces, like human organs or body surface, utilizing the BEM. The realistic human torso volume conductor is used in this study. The approximated solution $\tilde{\Phi}(r)$ is defined as a linear combination of N basis functions,

$$\tilde{\Phi}(r) = \sum_{i=1}^{N}\phi_i g_i(r), \tag{5}$$

with the constraint conditions for any point r on a surface: $\sum_{i=1}^{n} g_i(x) = 1$. The coefficients ϕ_i represent the values that are determined by constraining $\tilde{\Phi}(r)$ to satisfy Eq. (3) at discrete points, thereby generating a system of equations in ϕ_i.

Substituting the expression for Eq. (5) into Eq. (4), $B(r)$ can be rewritten as a linear combination of vector functions:

$$B(r) = B^{\infty}(r) - \sum_{i=1}^{n}\{\phi_i\boldsymbol{D}_i(r)\} \tag{6}$$

with the vector function given by

$$\boldsymbol{D}_i(r) = \frac{\mu_0}{4\pi}(\sigma_-^k-\sigma_+^k)\iint\limits_{\Delta_{i(j,k)}\in S_k} g_i(r')\nabla\Big(\frac{1}{|\boldsymbol{r}-\boldsymbol{r}'|}\Big)\times\mathrm{d}S''. \tag{7}$$

These vector functions are weighted by ϕ_i, which are obtained from the BEM solution to Eq. (3).[18] The surfaces S^k are tessellated with suitable triangular elements $\Delta_{i(jk)}$, which represent any triangle for the basis function g_i. Then, we use the vector identity and Stokes' theorem, and the discretized version of Eq. (7) can be written as[22]

$$\begin{aligned} \boldsymbol{D}_i(r) \;=\; & \frac{\mu_0}{4\pi}\sum_{i(jk)}\Big\{(\sigma_-^k-\sigma_+^k)\frac{\boldsymbol{r}-\boldsymbol{r}'}{2A_{i(jk)}} \\ & \times\Big[\sum_{p=1}^{3}[\boldsymbol{n}\cdot(\boldsymbol{c}_p\times\boldsymbol{c}_{p+1})\cdot\gamma_p^0] - (\boldsymbol{n}\cdot\boldsymbol{c})\cdot\Omega_{ijk}\Big]\Big\}, \end{aligned} \tag{8}$$

where $A_{i(jk)}$ denotes the areas of $\Delta_{i(jk)}$. Here the function γ_p^0 defined by De Munck[20] is redefined by

$$\gamma_p^0 = \frac{1}{|y_{p+1}-y_p|}\ln\Big(\frac{|y_{p+1}||y_{p+1}-y_p| + y_{p+1}\cdot(y_{p+1}-y_p)}{|y_p||y_{p+1}-y_p| + y_p\cdot(y_{p+1}-y_p)}\Big).$$

The coplanar vector $\boldsymbol{c}_p$ is normal to $\boldsymbol{c}$ and extends from A to each vertex of $\Delta_{i(jk)}$. A subscript p can be introduced to refer to points i,j,k for $p = 1,2,3$ respectively, and each point can be cyclically referenced using $p-1$ and $p+1$. $\Omega_{ijk} = \sum_{p=1}^{3}\Omega_{A,p,p+1}$ is the sum of the solid angles. $\boldsymbol{n}$ is the unit outward surface normal vector for Δ_{ijk}.

We obtain the final analytic solution for the magnetic field, so Eq. (3) can be written as

$$\begin{aligned} B(r) \;=\; & B^{\infty}(r) - \sum_{i=1}^{n}\Big\{\frac{\mu_0}{4\pi}\cdot\phi_i\sum_{i(jk)}\Big\{(\sigma_-^k-\sigma_+^k)\frac{\boldsymbol{r}-\boldsymbol{r}'}{2A_{i(jk)}} \\ & \times\Big[\sum_{p=1}^{3}[\boldsymbol{n}\cdot(\boldsymbol{c}_p\times\boldsymbol{c}_{p+1})\cdot\gamma_p^0] - (\boldsymbol{n}\cdot\boldsymbol{c})\cdot\Omega_{ijk}\Big]\Big\}\Big\}. \end{aligned} \tag{9}$$

3. Simulation and experiment

3.1. Simulation

The ECG and MCG simulation studies were performed based on the virtual heart electric model (LFX) with a spatial resolution of 1.5 mm, which was developed by Xia Ling's

group.[23] This anatomically and physiologically based model contains an atria-ventricular node, a His bundle, left and right bundles, and Purkinje fiber. In this simulation study, only the ventricular part was used. Once activation has reached the ventricles, propagation proceeds along the Purkinje fibers to the inner walls of the ventricles, and the resultant vector of the electric activity is illustrated with a thick arrow, therefore nine electro–cardiac vectors, each representing a segment of cardiac conduction of excitation, which are shown in Fig. 1(a), are located spatially at the centroid of the myocardial segment. The mesh of the torso volume conductor model is shown in Fig. 1(b).

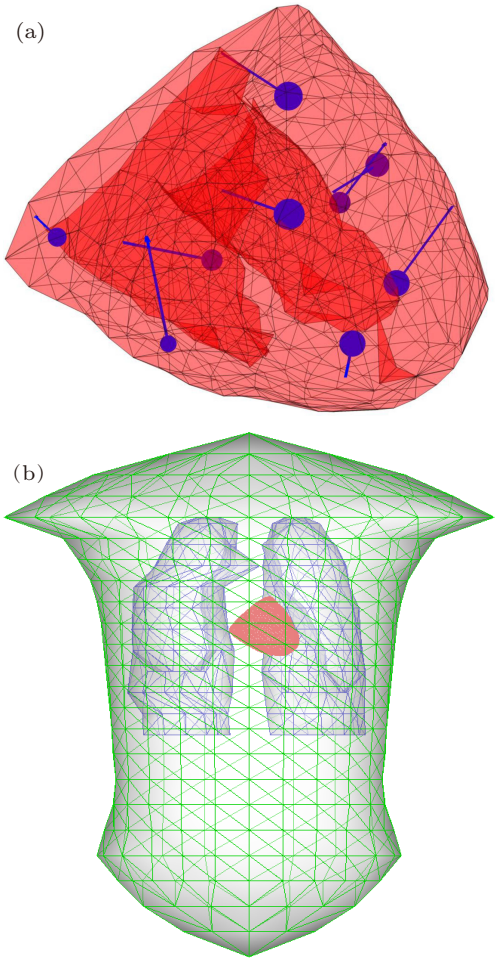


Fig. 1. (a) Nine distributed electro–cardiac vectors for cardiac equivalent sources based on the virtual heart and (b) realistic human torso volume conductor with lungs.

3.2. Experiment

We conducted our MCG measurements in a magnetically shielded room using a compound four-channel HT_c·SQUID system. The magnetic field sensitivity of all channels is above 100 fT·Hz$^{-1/2}$. The sensors of HT_c·SQUID are arranged in a 6×6 grid with a length of 40 mm, giving a measurement area of 200 mm $\times$ 200 mm. The plane of observation (Fig. 2) above the chest is considered to be the x–y plane, where x and y are the axes, with x going from right to left and y going from head to foot. The signals at each recording site, which can be freely input, are acquired at a sampling rate of 1 kHz with a power-line noise (50 Hz) filter. The measurement recording time is 30 s–100 s.

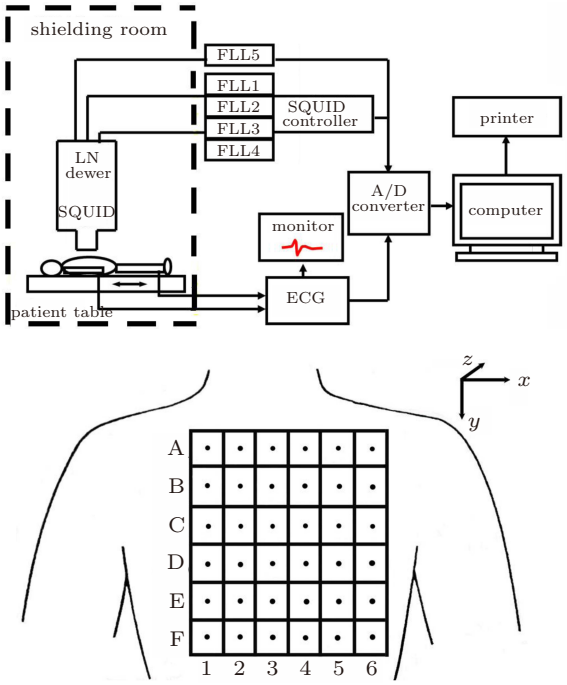


Fig. 2. Measurement area and 6×6 recording sites on the chest.

4. Results and discussion

The simulated 12-lead ECGs and MCG are obtained by the nine-vector cardiac model based on a virtual heart in a realistic human torso, with internal inhomogeneities, including the shape and resistivity of the lungs.

Time intervals (QRS and QT times) and wave amplitudes are calculated using a computer. R-wave amplitudes, QRS voltage, and Q-wave amplitudes were measured in millivolts. They were found to be well within the range of normal as seen in Fig. 3. This serves to validate MCG further.

The simulated plane is parallel to the chest, the distance between them is 40 mm, according to our measurement system for MCG. A map of MCG is shown for both the magnetic analog of the QRS wave and the T wave. Compared with the 12-lead ECG, it is found that the simulated MCG does not differ significantly from aVF, V4, V5, V6, I, II, and III in simulated 12-lead ECGs, the rest of which has obvious negative-going S wave. Using this model, we have conducted a preliminary study. We will calculate a series of MCG mappings based on a whole-heart model in the future.

In addition, the simulated MCG is compared with the measured MCG in D4 of a normal male. The simulated results can well reproduce the major features of an actual MCG signal, such as magnitude and durations. The former has the same wave forms as the latter from 400 ms to 900 ms, and we can see that the simulated MCG has no P wave because the cardiac vector model does not include atria. We also find

that the curves of the measured MCG are not smoother than those from the simulated MCG; the main reason for this result is related to external noise, such as the Earth's magnetic field and space's electromagnetic field. Besides the absence of an analog to the P wave, the factor most noticeable in the map is amplitude of MCG, which is a physically significant characteristic of the current system in the heart and its vicinities. Both of them are 65 pT approximately.

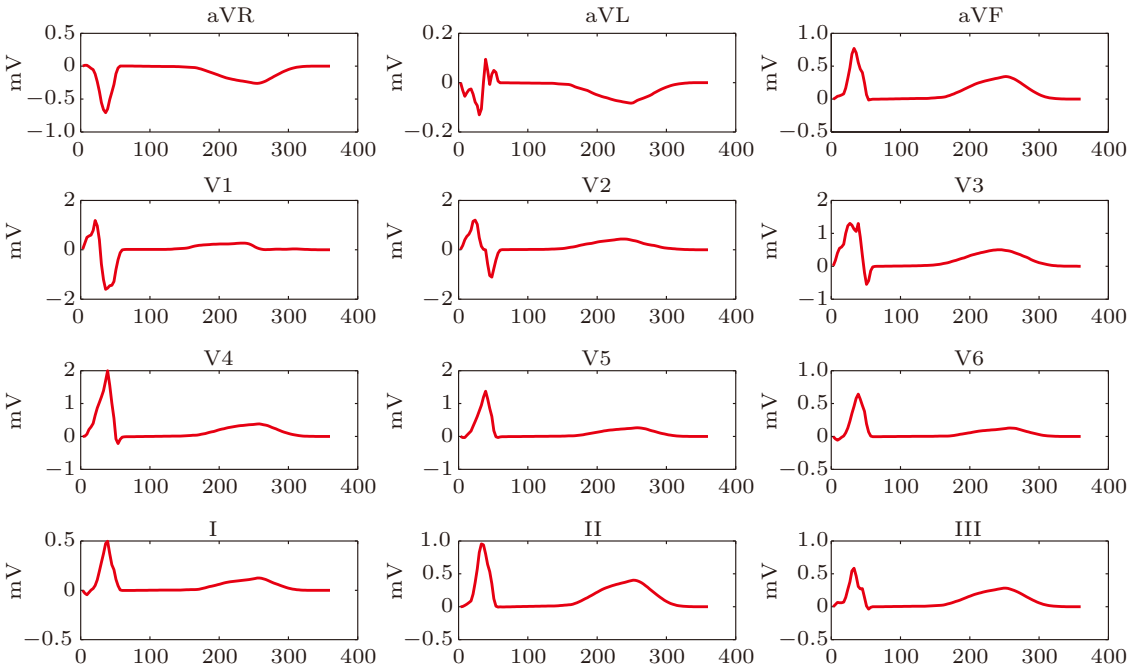


Fig. 3. Simulated 12-lead ECG, normal torso with lungs, the unit of coordinates x is ms.

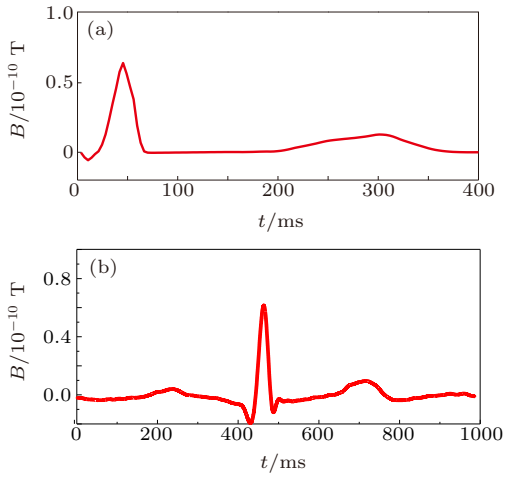


Fig. 4. Simulated MCG generated by the 9 electro–cardiac vectors, (b) measured MCG mapping in D4 of normal male using SQUID.

One way of describing cardiac activation is to plot the sequence of instantaneous depolarization wavefronts. In the presented data, the contributions of this cardiac generator during ventricular depolarization (QRS) are simulated for the total body surface isopotential map and 2D isomagnetic map of MCG. Figure 5 shows instantaneous pictures for the R wave of the BSPM and the MCG. The surface connects all points in the same temporal phase, the wavefront surface is also referred to as an isochrone.

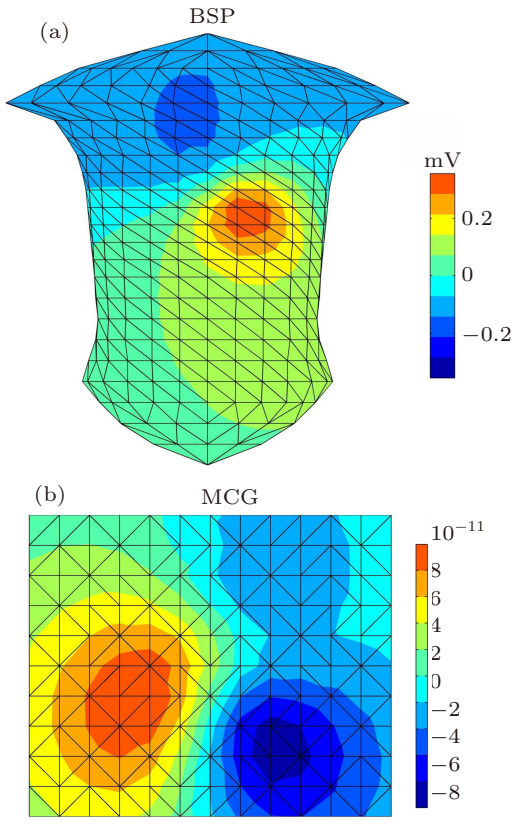


Fig. 5. For $t = 40$ ms (a) body surface isopotential map for R wave and (b) 2D isomagnetic map for R wave on the plane parallel to the torso model.

As in the case of the BSPM and the 2D isomagnetic map, it is found that the magnetic field can be approximated by multiple vectors fixed in position but variable in magnitude and orientation. The 2D isomagnetic map is very complex: multiple satellite minima or maxima come and go and the null line is also complex and not a straight line. However, we can still obtain extra information for the activated dipole from the maxima and minima nodes, such as orientation.

The BSPM and the 2D isomagnetic map of the MCG are the imaging diagnosis methods. In contrast to BSPM, the MCG is more localized in that measureable magnetic fields exist only near large currents. For example, the MCG does not need to be simulated in the whole human torso volume conductor. Another crucial difference between the MCG and the BSPM is that the MCG is dependent only on the transport of charge within the body, and totally independent of the resistive characteristics of the medium outside of the body, which makes it easy to visualize the electrophysiological behavior of the heart.

5. Conclusion

In this paper, we present a cardiac vector model and test this model using the experimental results obtained from the compound four-channel HT_c·SQUID systems in a magnetically shielded room, and then discuss the forward problem for cardiac magnetic fields and electric potential based on this model and the realistic human torso volume conductor model. Compared with experimental results, some meaningful results are obtained, which have vital significance for guiding MCG research and applications.

Further research is needed to establish a new cardiac vector model, such as a high-precision virtual whole-heart model. The new model will allow for the study of complex combinations of myocardial infarctions (ST waves), chamber hypertrophy, abnormalities of myocardial conduction, and so on. Meanwhile, this anatomically and physiologically based model will, when properly validated, provide a rational basis for a methodical exploration of parameters in the torso, such as variations in torso shape, inhomogeneities, and the size and location of the heart, which might influence an MCG.

References

[1] Cohen D and Hosaka H 1976 *J. Elektrocard.* **9** 409
[2] Erne S N 1985 *Med. Biol. Eng. Comput.* **23**(S2) 1447
[3] Makijarvi M, Nenonen J, Leinio M and Montonen J 1992 *J. Electrocardiology* **25** 143
[4] Ma P, Yao K, Xie F X, Zhang S Y, Deng P, He D F, Zhang F, Liu L Y, Nie R J, Wang F R, Wang S Z and Dai Y D 2002 *Acta Phys. Sin.* **51** 224 (in Chinese)
[5] Tsukada K, Kandori A, Miyashita T, Sasabuti H, Suzuki H, Kondo S, Komiyama Y and Teshigawara K 1998 *IEEE Eng. Med. Biol. Soc.* **20** 524
[6] Schlitt H A, Heller L, Aaron R, Best E and Ranken D M 1995 *IEEE Trans. Biomed. Eng.* **42** 52
[7] Gencer N G and Tanzer I O 1999 *Phys. Med. Biol.* **44** 2275
[8] Fuchs M, Kastner J, Wagner M, Hawes S and Ebersole J S 2002 *Clin. Neurophysiol.* **113** 702
[9] Akalın-Acar Z and Gencer N G 2004 *Phys. Med. Biol.* **49** 5011
[10] Tang F K, Wang Q, Hua N, Tang X Z, Lu H and Ma P 2010 *Chin. Phys. B* **19** 120601
[11] Johnson C R 1997 *CRC Crit. Rev. Biomed. Eng.* **25** 1
[12] Güllmar D, Reichenbach J R, Anwander A, Knösche T, Wolters C H and Eiselt M 2005 *Int. J. Bioelectromagnetic* **7** 108
[13] Lemieuxy L, McBride A and Hand J W 1996 *Phys. Med. Biol.* **41** 1079
[14] Wang Q, Ma P, Lu H, Tang X Z, Hua N and Tang F K 2009 *Chin. Phys. B* **18** 5566
[15] Zhang L, Jiang S Q, Wang L, Luo M and Wang Y M 2005 *Modern Scientific Instruments* **4** 31 (in Chinese)
[16] Malmivuo J 1995 *Bioelectromagnetic*, Vol. 8 (New York: Oxford University Press) p. 148
[17] Sarvas J 1987 *Phys. Med. Biol.* **32** 11
[18] Shou G F, Xia L, Jiang M F, Wei Q, Liu F and Crozier S 2009 *IEEE Trans. Biomed. Eng.* **1454** 52
[19] Geselowitz D B 1970 *IEEE Trans. Magn.* **MAG-6** 346
[20] Cuffin B N and Cohen D 1977 *IEEE Trans. Biomed. Eng.* **BME-24** 372
[21] Stenroos M, Mantynen V and Nenonen J 2007 *Comput. Methods Programs Biomed.* **88** 256
[22] Ferguson A S, Zhang X and Stroink G 1994 *IEEE Trans. Biomed. Eng.* **41** 455
[23] Xia L 1995 "A New Approach to Electrcardiographic Inverse Problem Studies: Solution in Terms of Heart-torso Model Parameters", Ph. D dissertation, (Hangzhou: Zhejiang University) (in Chinese)
[24] Lu W X and Xia L 1996 *IEEE Trans. Biomed. Eng.* **43** 211